DIFFUSE COMPONENT SPECTRA OF SOLAR ACTIVE REGIONS AT SUBMILLIMETER WAVELENGTHS

ADRIANA V. R. SILVA[1], TATIANA F. LAGANÁ[1,2], C. GUILLERMO GIMENEZ DE CASTRO[1], PIERRE KAUFMANN[1,3], JOAQUIM E. R. COSTA[1,4], HUGO LEVATO[5] and MARTA ROVIRA[6]

[1]*CRAAM, Universidade Presbiteriana Mackenzie, Rua da Consolação, 896, São Paulo, SP 01302-907, Brazil*

[2]*Instituto de Física, Universidade de São Paulo, São Paulo, SP, Brazil*

[3]*CCS, UNICAMP, Campinas, São Paulo, SP 13083-970, Brazil*

[4]*Instituto Nacional de Pesquisas Espacias, INPE, São José dos Campos, SP, Brazil*

[5]*Complejo Astronómico El Leoncito, Casilla de Correo 467, Av. España 1512 Sur, San Juan 5400, Argentina*

[6]*Instituto de Astronomia y Física del Espacio, Casilla de Correo 67, Sucursal 28, Buenos Aires 1428, Argentina*

(e-mail: asilva@craam.mackenzie.br)

Abstract. Solar maps at 212 and 405 GHz obtained by the Solar Submillimetric Telescope (SST) show regions of enhanced brightness temperature, which coincide with the location of active regions. A statistical study of the radio emission from these active regions was performed for the first time at such high frequencies during 23 days on June and July 2002, when the atmospheric opacity was low. The brightest regions on the maps were chosen for this study, where the brightness excess observed varies from 3 to 20% above quiet Sun levels (i.e., $200-1000$ K) at both wavelengths. Sizes of the regions of enhanced emission calculated at half the maximum value were estimated to be between $2'$ and $7'$. These sizes agree with observed sizes of active regions at other wavelengths such as Hα and ultraviolet. An important result is that the flux density spectra of all sources increase toward submillimeter frequencies, yielding flux density spectral index with an average value of 2.0. The flux density of the active region sources were complemented with that from maps at 17 and 34 GHz from the Nobeyama Radio Heliograph. The resulting spectra at all four frequencies were fit considering the flux density to be due to thermal bremsstrahlung from the active region. In the calculations, the source radius was assumed to be the mean of the measured values at 212 and 405 K. The effective temperatures of the radio emitting source, assumed homogeneous, obtained from this fit were $0.6-2.9 \times 10^4$ K, for source diameters of $2'-7'$.

1. Introduction

Raster scans maps of the Sun at radio frequencies obtained since the early 1960s have shown the existence of regions of enhanced brightness temperature on the solar disk. These regions of higher brightness temperature were found to be associated with Hα active regions, sunspots, plages, and regions of strong magnetic fields (Simon, 1965; Hachenberg, Steffen, and Harth, 1978; Bastian, Ewell,

and Zirin, 1993). Since the emission at short wavelengths originates mainly from the chromosphere, observations of high-frequency radio emission from active regions may provide valuable information on the atmosphere above active regions on the Sun. These observations provide crucial information for models of the solar atmosphere.

The active-region-associated component of the solar emission has been measured at many wavelengths from microwaves to far infrared (50 μm). Active region emission spectra at radio microwave wavelengths, due to gyro-resonance of thermal electrons, were found to peak at 2–5 GHz (Kakinuma and Swarup, 1962), whereas the emission at higher frequencies was attributed to thermal bremsstrahlung (Kundu, 1970).

A compilation of past results from radio observations of active regions is presented in Table I. In this study we concentrate on millimetric and submillimetric observations. From the results summarized in the table, it is seen that the brightness temperature enhancements are a few hundred kelvin, which is within a few percent of the quiet-Sun value. The excess brightness temperature values do not exceed 6% for measurements above 200 GHz (we point out that the Bastian, Ewell, and Zirin (1993) values were obtained after deconvolution of the maps). From 10 to 100 GHz, the observed sizes of the extended radio sources range from 1$'$ to 7$'$.

Two types of radio sources were identified in active regions at 10.7 GHz (Tapping and Zwaan, 2001). The diffuse sources, with sizes larger than 40$'$, low-brightness temperatures ($\sim 2 \times 10^4$ K), and densities of 1–2 $\times$ 10^9 cm^{-3}, were found to be due to thermal emission and were associated with plages. On the other hand, the compact sources with sizes less than 40$''$, had high-brightness temperatures ($\sim$10^6 K), and were associated with sunspots. Moreover, their emission was seen to vary with position on the solar disk. In this case, the emission spectra are thought to be thermal gyro-resonance emission related to strong magnetic fields ($B \sim$ 1300 G; Tapping and Zwaan, 2001). A few of the brighter compact sources were believed to be due to non-thermal gyro-synchrotron emission from the sources associated with complex magnetic field regions (δ spots) with high flaring activity.

Even though active regions have already been detected sporadically at submillimeter frequencies, no statistical analysis on the flux density spectra of several observed sources has been done at these high frequencies, which is the goal of the present work. In order to better understand the spectral behavior of the active region emission, we have also included millimetric maps in this analysis. In the next section, the millimetric and submillimetric data are presented. This section reports the study of the brightness temperature enhancements associated with active regions at 212 and 405 GHz, and the results from the 17 and 34 GHz maps. The spectra of the active regions are discussed in Section 3. Finally, the discussion and conclusions are presented in the last section.

TABLE I

Active region observations.

ν (GHz)	T_B (K)[a]	ΔT (K)[b]	$\Delta T/T_B$ (%)	Size (′)	Reference
10.7		$1-6 \times 10^4$		$2-7$	Tapping and Zwaan (2001)
15, 35, 70, 100			$5-10$	$2-5$	Tlamicha (1968)
33	7000	$200-600$	14	$2-6$	Kundu (1970)
35	9500	$50-250$	$1-3$	$0.5-0.9$	Hachenberg, Steffen, and Harth (1978)
37	7500	$200-2000$	$3-30$	$2-7$	Efanov *et al.* (1969)
37	8000	$540-2040$	$7-25$		Efanov, Kislyakov, and Moiseev (1972)
50	7300	$500-1180$	$7-16$		Efanov, Kislyakov, and Moiseev (1972)
75	7000	$400-840$	$6-12$		Efanov, Kislyakov, and Moiseev (1972)
85	6400	700	11		Buhl and Tlamicha (1970)
86	6400	$100-600$	11	$1-5$	Kundu (1970)
94	6400	$200-300$	$1-2$		Simon (1965)
133	5600	$350-1050$	$6-19$	$1-10$	Efanov *et al.* (1969)
150	6000	$350-800$	$6-13$		Efanov, Kislyakov, and Moiseev (1972)
250	6000	150	3		Kundu (1970)
250	5600	350	6		Beckman and Clark (1973)
353	5580	600	11		Bastian, Ewell, and Zirin (1993)
375	5000	300	6		Beckman and Clark (1973)
750	4600	200	4		Beckman and Clark (1973)
$300-857$			$5-20$		Righini-Cohen and Simon (1977)
670, 857	4500	$45-90$	$1-2$		Righini and Simon (1976)
1500	4475	250	6		Degiacomi *et al.* (1984)
3750	4500	200	4		Degiacomi *et al.* (1984)
6000		125			Degiacomi *et al.* (1984)

[a]Brightness temperature of quiet-Sun level.
[b]Excess brightness temperature above quiet-Sun level.

2. Observational Data

2.1. SUBMILLIMETRIC OBSERVATIONS

During a period of over 2 months in 2002, daily maps of the Sun were made with the Submillimetric Solar Telescope (Kaufmann *et al.*, 2001) at 212 and 405 GHz. These

maps were composed of 31 raster scans in azimuth (with data taken every 30″) with shifts in elevation, separated by 120″. It takes less than 5 min of observation for each map. The widths of the beams are approximately 4′ and 2′ at 212 and 405 GHz, respectively. From these, a total of 23 maps were chosen during days when the atmospheric opacities were low ($\tau_{212} < 0.2$ and $\tau_{405} < 1.2$). No flares occurred during the observation of these maps. In order to complement our analysis, in this study we have also included maps of the same days from the Nobeyama Radio Heliograph (NoRH) at 17 and 34 GHz.

The dates of observations and the active regions under consideration are listed in Table II. For each observation day, we have chosen the brightest active region

TABLE II
Active regions.

Date	Position[a]	NOAA AR	ΔT_{212} (K)[b]	ΔT_{405} (K)[c]
23 May 2002	N05W05	9957	890	830
30 May 2002	S02E15	9970	360	290
7 June 2002	S11E15	9987	440	300
8 June 2002	S15E02	9981	430	610
10 June 2002	S15W05	9987	420	640
13 June 2002	S17E12	9992	330	400
14 June 2002	S15E03	9992	440	340
15 June 2002	N05E35	9997	550	840
16 June 2002	N04E16	9997	900	1060
17 June 2002	N04E15	9997	1020	1070
19 June 2002	N11W04	0000	900	610
20 June 2002	N11W10	0007	780	710
23 June 2002	S03E02	0008	550	620
28 June 2002	S17E01	0017	430	290
29 June 2002	S13E25	0016	270	490
7 July 2002	S21W00	0023	570	500
13 July 2002	N14E26	0030	900	840
17 July 2002	N07W04	0030	650	970
18 July 2002	N04W11	0030	510	730
21 July 2002	S19E07	0036	500	630
25 July 2002	N07E13	0045	440	530
26 July 2002	S24E22	0039	440	850
28 July 2002	S25W07	0039	570	850

[a]Heliographic coordinates at 0 UT.
[b]Excess brightness temperature above quiet-Sun level (5900 K) at 212 GHz.
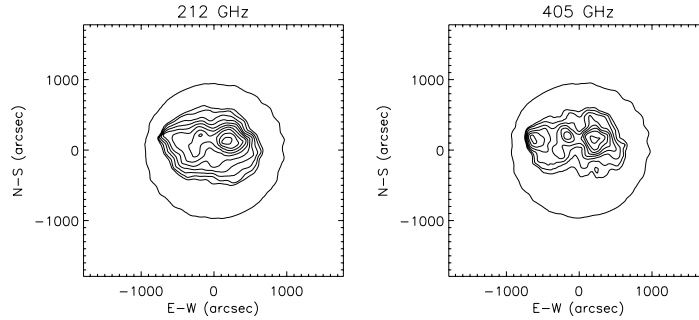[c]Excess brightness temperature above quiet-Sun level (5100 K) at 405 GHz.

Figure 1. Example of solar maps at 212 and 405 GHz obtained on 19 June 2002. Contour levels are 50, 99, 100, 101, 102, 103, 104, 105, 106, 107, 108% of the quiet-Sun level.

observed at 212 GHz by SST. Examples of such maps are shown in Figure 1, the maps have been rotated such that solar north is up, and west is to the right. On these maps, the regions under study can be seen as small enhancements of 3 – 20% above the quiet-Sun level.

The brightness temperature of the quiet Sun, and consequently of the active regions, were calibrated against observations of the new moon. The new moon brightness temperatures adopted in this calculation were 125 and 102 K (Linsky, 1973), at 212 and 405 GHz, respectively, whereas the quiet-Sun level was determined as the most common value of the map. This quiet-Sun brightness temperature was corrected so as to match the solar brightness values calibrated according to observations of the new moon performed with SST at 212 and 405 GHz, where the total signal deflection of the Sun equaled 5900 and 5100 K, respectively. Thus, these values were taken as the quiet-Sun brightness temperature at 212 and 405 GHz.

The brightness temperature of the active regions, T_b, was obtained by correcting for the beam efficiency at both frequencies $T_b = T_a/\eta$, since the active region sizes are of the order of the beam size (a few arcmin), where T_a is the measured antenna temperature. The beam efficiency, η, as defined by Mangum (1993) was estimated using NoRH 17 GHz maps as models of the active region morphology due to the higher angular resolution. A 17 GHz map, with $10''$ spatial resolution, was convolved with the actual SST beams, which were obtained from tomography reconstruction techniques (Costa *et al.*, 2002). The flux density of these convolved maps was then calculated by adding the values within all the pixels of the region (in an area larger than twice the size of the beam) and compared with the value before the convolution. The beam efficiency results obtained this way were 58 and 53% at 212 and 405 GHz, respectively. These values agree with those estimated directly from the beam shape, considering only the main lobe.

The excess brightness temperature above quiet-Sun values, ΔT_b, was estimated considering the above beam efficiency values. The maximum brightness
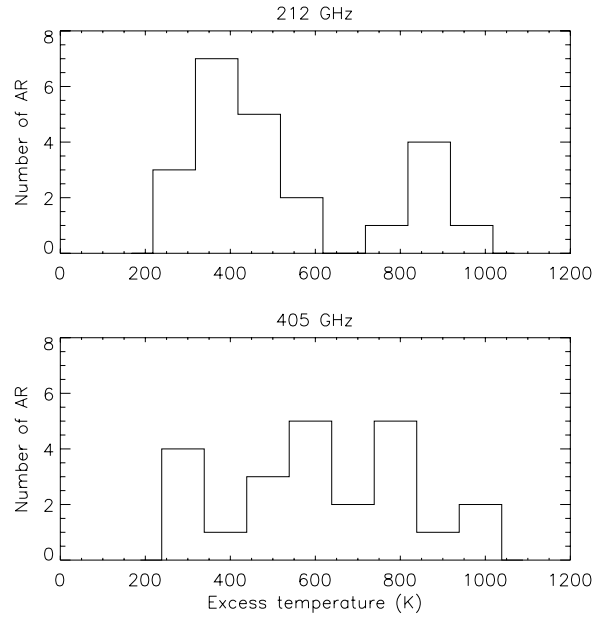
Figure 2. Histogram of the excess brightness temperature above quiet-Sun values at 212 GHz (*top panel*) and 405 GHz (*bottom panel*).

temperatures enhancements for the active regions studied are listed in Table II. A mean value for $\Delta T / T_b$ of 10 and 13% was obtained for the active region emission at 212 and 405 GHz, respectively.

Histograms of the excess brightness temperature at both wavelengths are shown in Figure 2, the 212 GHz results are shown in the top panel, whereas the 405 GHz results are shown in the bottom panel. At both wavelengths, the excess brightness temperatures values range from 200 to 1000 K, with mean values of 580 and 650 K at 212 and 405 GHz, respectively. No dependency of the intensity on heliocentric angle was found for the active regions that were observed on more than 1 day.

The sizes of the regions have also been estimated as that where the values of emission falls to half its maximum value. Assuming a Gaussian shape for the source, the observed width at half-power, θ_o, is the result of the real source size, θ_s, convolved with the beam, θ_b, also assumed to have a Gaussian shape. Thus, the actual source size at half intensity is given by $\theta_s = \sqrt{\theta_o^2 - \theta_b^2}$. The sizes have been computed in the east–west and north–south directions, and the diameter of the source taken as the mean of both values. The size of one of the observed active regions could not be determined because the observed diameter was equal to the beam size. A histogram of the 22 active region mean diameters at half the maximum intensity is shown in Figure 3 for both frequencies. As can be seen from the figure, the sizes are approximately the same at both frequencies, and their values range from 2′ to 7′ with a mean of 4.6′ ± 2.1′ at 212 GHz, and 4.9′ ± 1.4′ at 405 GHz.
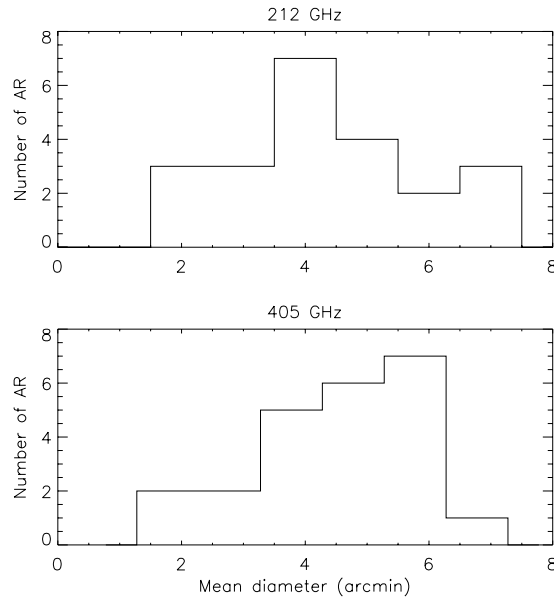
Figure 3. Histogram of mean diameter of the active regions at 212 GHz (*top panel*) and 405 GHz (*bottom panel*).

These sizes are slightly larger than the beam size at 212 GHz, and probably represent the diameter of several sources within an active region complex. In this case, the brightness temperature enhancements represent an average value of the multiple active region sources.

2.2. MILLIMETRIC OBSERVATIONS

In order to complement these results and to estimate the effective temperature and density of the emitting region from the flux density spectra, we have compared the SST maps with data at lower frequencies. For that, we have included in the analysis maps of the same days from the Nobeyama Radio Heliograph at 17 and 34 GHz, assuming that there were no substantial changes in the active region emission within the 12-h time interval between observations. Since this instrument is an interferometer, the spatial resolution of the maps at these frequencies is much higher, being 10$''$ and 5$''$ at 17 and 34 GHz, respectively (Nakajima *et al.*, 1994). In order to work with the same resolution, the 34 GHz maps were convolved with the 17 GHz beam using the NoRH software available from the Solar Software Package.

Examples of the Nobeyama maps are shown in Figure 4 in the top two panels for 17 GHz (left) and 34 GHz (right). On the bottom of the same figure are also displayed maps at 212 GHz (left) and 405 GHz (right). The active region selected, the brightest one at 212 GHz, is within the square box, 7$'$ on the side, drawn on
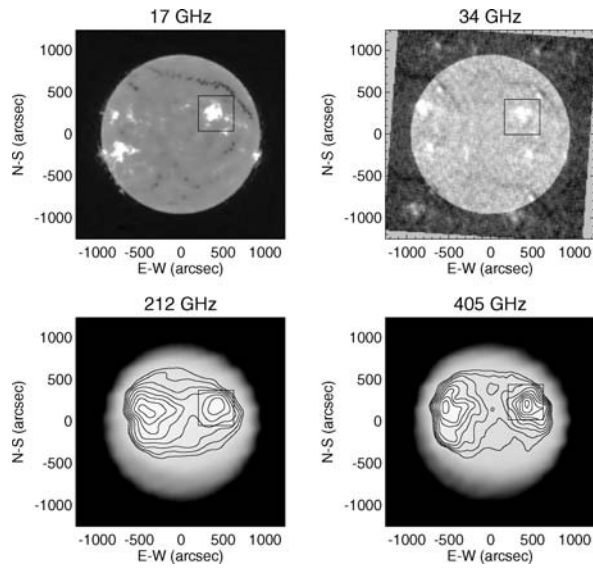
Figure 4. Maps of the Sun at 17, 34, 212, and 405 GHz obtained on 18 July 2002. Contour levels at 212 and 405 GHz are 99, 100, 101, 102, 103, 104, 105, 106, 107% of the quiet-Sun level.

the figure. The excess brightness temperatures above the quiet-Sun level for the same active regions in the millimeter maps were calculated for the 23 days listed in Table II.

2.3. OPTICAL AND ULTRAVIOLET IMAGES

Images at other wavelengths, other than microwaves, were obtained in order to compare with the submillimetric maps. These images were obtained from the Active Region Monitor homepage maintained by the Big Bear Solar Observatory (BBSO). Here, these images are used only to define the boundaries of the magnetic structure that define the active region, because for each wavelength the level of emission differs, and so do the plasma parameters. As an example, we use the active region, on 18 July 2002, depicted in Figure 4, when the SST was tracking active region 0030. Some of the observations at Hα and ultraviolet wavelengths of this active region plus a magnetogram are shown in Figure 5.

On this day, the size of this active region was measured to be 5.4$'$ and 4.3$'$ at 212 and 405 GHz, respectively. As can be seen from Figure 5, these sizes are compatible with the east–west extension of the active region magnetogram (top left). In order to check if this size is compatible with that of the Hα and ultraviolet images of the active region, we have convolved the images with a Gaussian of 4$'$ FWHM (the same width of the 212 GHz beam). The actual size of the active region in the degraded image is then obtained in the same way as with the submillimetric
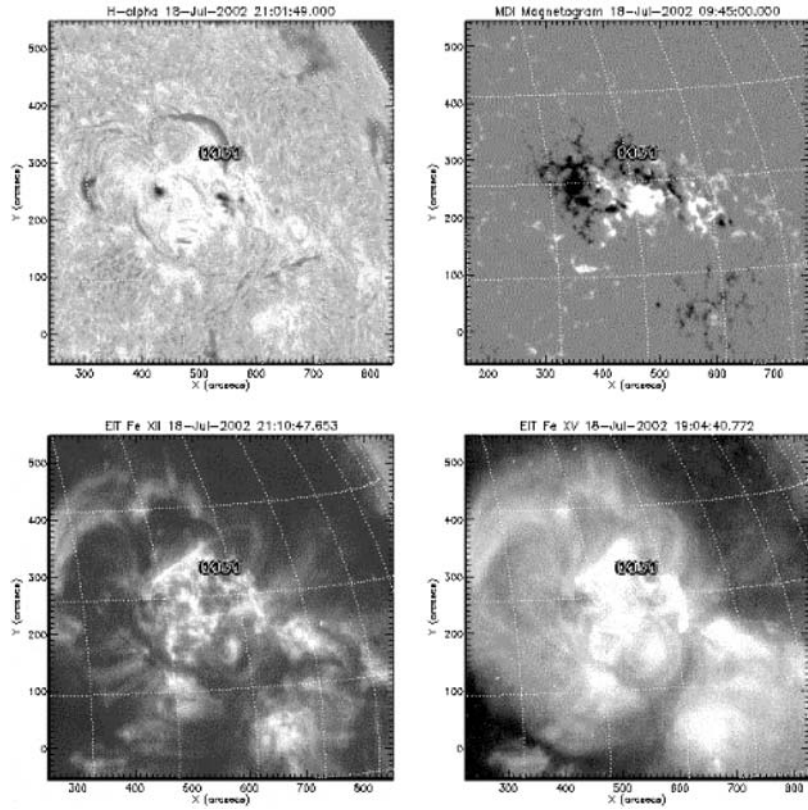
Figure 5. Images of the Sun at 18 July 2002. *Upper right*: MDI magnetogram; *upper left*: Hα from BBSO; *lower panels*: ultraviolet from EIT.

maps, that is, $\theta_s = \sqrt{\theta_o^2 - \theta_b^2}$. For the Hα active region, we obtain $\theta_o = 6.2$, resulting in $\theta_s = 4.7'$. This is a measure of the excess emission due to the plage area. As for the Fe XII ultraviolet image, the measured size of the convolved active region was $7.1'$, implying an actual size of $5.8'$. These sizes are in good agreement with those measured from the submillimetric data.

3. Active Region Spectra

The brightness temperature of the active regions at all frequencies can be converted to flux density, S_ν, using the Rayleigh–Jeans approximation for a homogeneous source, $S_\nu = 2K_B T_b \Omega_s / \lambda^2$, where K_B is the Boltzmann constant, λ the wavelength, and Ω_s the source solid angle. The brightness temperatures of the active regions at 212 and 405 GHz were estimated by correcting for the main beam efficiency as explained before. Then, the flux densities were calculated at all frequencies as the

sum of all T_b values within a box of $7'$ in size. Thus, according to the Rayleigh–Jeans approximation:

$$S_\nu = \frac{2K_B}{\lambda^2} \theta_{\text{pix}}^2 \sum_{\text{box}} T_b, \tag{1}$$

where θ_{pix} is the angular size of the map pixel in radians and the summation is performed over all pixels within the box.

3.1. EXCESS FLUX DENSITY SPECTRA

In order to compare with previous results in the literature, the flux densities, ΔS, associated with the excess brightness temperature above quiet Sun values were calculated using $T_b = \Delta T_b$ in Equation (1). Figure 6 summarizes the excess flux density spectra, where the data discussed here are represented by crosses. For comparison, spectra of previous works are also plotted in the figure. The high-frequency observation of Efanov *et al.* (1969, asterisks), a mean value of a week long observation during 1967, also shows an increase in the flux density spectra, probably from an optically thick thermal source. The Efanov, Kislyakov, and Moiseev (1972, diamonds) and the Tsuchiya and Takahashi (1968, squares) data appear to have a similar behavior. The mentioned emission mechanisms are compact gyro-resonance emission at lower frequencies and diffuse optically thick thermal free–free emission at higher frequencies. It is necessary to add optically thin/thick thermal free–free emission from transition region and corona at millimeter or longer wavelengths. The high-frequency source is probably of the same type as the submillimeter sources
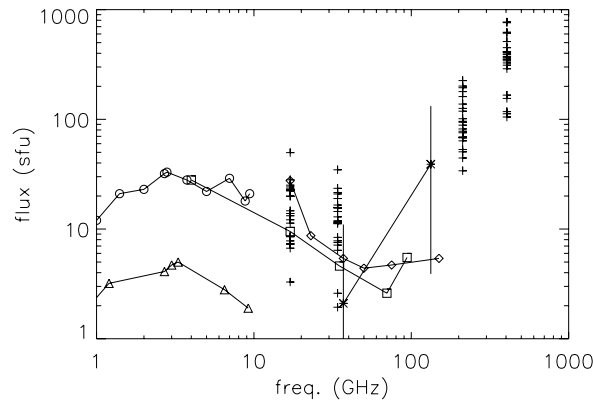

Figure 6. Comparison of submillimeter active region flux density spectra with previously published data. The *diamonds* represent Efanov, Kislyakov, and Moiseev (1972) data, the *asterisk* Efanov *et al.* (1969) observations, while Tsuchiya and Takahashi (1968) observations are indicated by *squares*. Eclipse data are represented by *triangles*, from Castelli and Clemens (1966), and by *circles* (Kaufmann, 1968). The *crosses* represent the submillimeter and millimeter observations discussed in the text.

discussed in the previous sections. On the other hand, both Castelli and Clemens (1966, triangles), and Kaufmann (1968, circles) eclipse observations at frequencies <10 GHz, appear to be due to gyro-resonance emission.

To infer the emission mechanism at high radio frequencies, we may estimate the flux density spectral index, α, from the 212 and 405 GHz observations since $S_\nu \sim \nu^\alpha$. The indices can be roughly estimated from the active regions excess brightness temperatures, assuming their sizes are the same at the two high frequencies. First, the maximum intensity within each active region under consideration was normalized to the quiet Sun value of the map, and then multiplied by the solar brightness temperature of 5900 and 5100 K at 212 and 405 GHz, respectively. Next, in order to obtain the brightness temperature excess of the active region, we have subtracted the brightness temperature of the quiet Sun, that is 5900 and 5100 K, respectively, yielding estimates of the maximum brightness temperature excess of the active regions, ΔT_{212} and ΔT_{405}. Finally, the spectral index was calculated as

$$\alpha = \frac{\log\left[\frac{\Delta T_{212}}{\Delta T_{405}}\left(\frac{212}{405}\right)^2\right]}{\log(212/405)}, \tag{2}$$

where the sizes of the active regions at the two frequencies were assumed to be the same, which is in agreement with the measurements presented in Figure 3. A histogram of the spectral index α for all active regions plotted in Figure 7 indicates that the flux density for all active regions increases with frequency, $i.e.$, $\alpha > 0$. These spectral indices with average value near to 2 suggest that the emission mechanism at submillimeter wavelengths may be due to thermal free–free emission from optically thick sources.
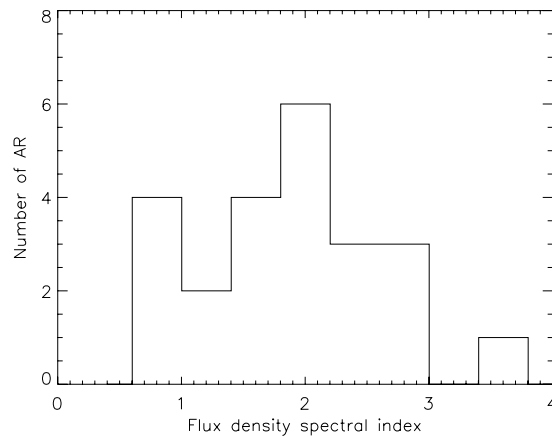

Figure 7. Histogram of 212–405 GHz flux density spectral index values calculated from the maximum brightness temperature excess.

3.2. TOTAL FLUX DENSITY SPECTRA

Since the sizes of the emission from 17 to 405 GHz roughly fill the telescope beams, the total observed emission probably originates from the active region. Thus, the active region flux density spectrum is determined using the total T_b measured, without subtraction of the background. The flux densities measured at the four frequencies for all active regions are shown as vertical bars in the panels of Figure 8. The uncertainty of the submillimeter flux density is of the order of 30%.

Based on the positive slope of the submillimetric spectra, a fit to the data, for the frequencies 17, 34, 212, and 405 GHz, for each active region was performed assuming free–free emission from a single optically thick isothermal source. In this case, the flux density is proportional to the effective temperature, the source solid angle, and the frequency squared. For a homogeneous circular Gaussian source of FWHM $= 2a$, the source solid angle is $\Omega_s = \pi(a/d_{sun})^2/\ln(2)$, where d_{sun} is the
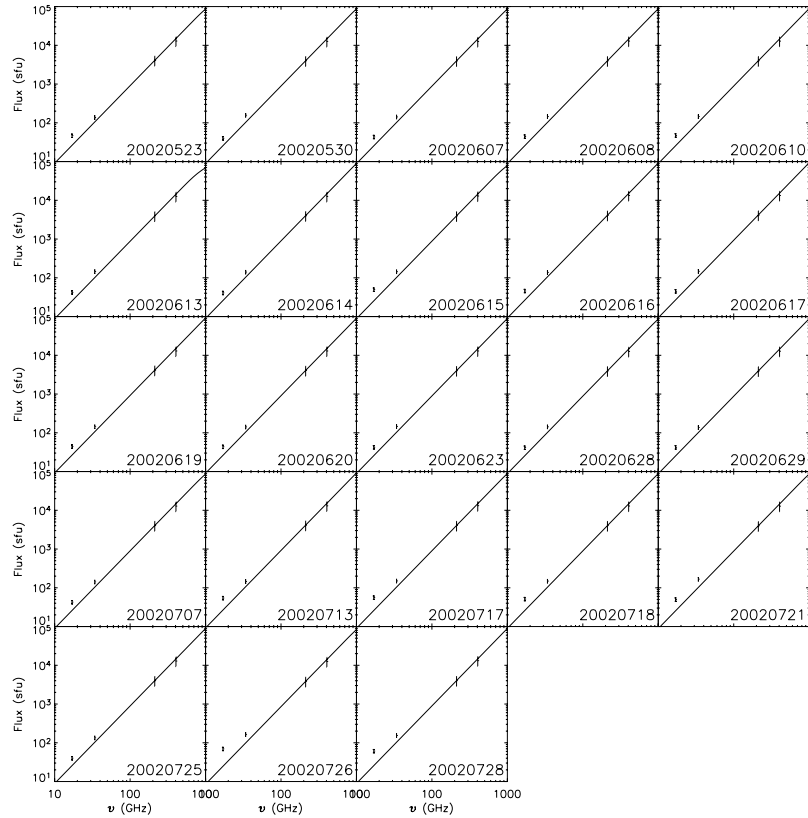

Figure 8. Total flux density spectra of the 23 active regions listed in Table II. The *solid line* represents the fit to the flux density, assuming the source to be optically thick.

Sun–Earth distance. The ln(2) factor appears because a is the source FWHM/2 and not the Gaussian width, σ.

The quadratic least-squares fit to the spectra of all active regions is also shown as a solid line in Figure 8. As is shown in Figure 8, millimetric emission (17 and 34 GHz) exceeds systematically the expected fluxes from the optically thick emission. This is partly due to gyro-resonance emission (17 GHz, Castelli and Clemens, 1966; Kaufmann, 1968; Tapping and Zwaan, 2001), due to optically thick thermal free–free emission from the upper chromosphere, and due to optically thin transition region and coronal sources.

From these fits it is possible to obtain the effective temperature, T_{ef}, considering the radius of the radio source, a, as the mean of the measured values at 212 and 405 GHz. A histograms of the effective temperature is shown in Figure 9.

As can be seen from the values plotted in Figure 9, the isothermal source effective temperature obtained is in the range $0.6–2.9 \times 10^4$ K, for source diameters of $2'–7'$. The fitted effective temperatures are higher than the observed brightness temperature, which is the same as the effective temperature for an optically thick source. One should bear in mind, however, that the active region sizes used in the fit are the deconvolved values, therefore, the fitted T_{ef} probably reflects the maximum deconvolved brightness temperature, which is expected to be larger than the observed one convolved with the telescope beam.

Since it appears that the emission at all frequencies is from an optically thick source, it is not possible to estimate the source density. If, however, one considers that the optical depth at 405 GHz is equal to unity, that is, $\tau_{405} = 1$, then it is possible to obtain lower-limit values to the density. The optical depth is approximated by
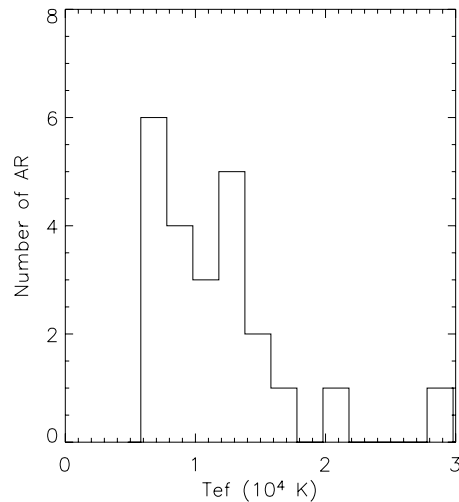

Figure 9. Effective temperature obtained from the free–free emission fit to the active region spectra for all four frequencies.
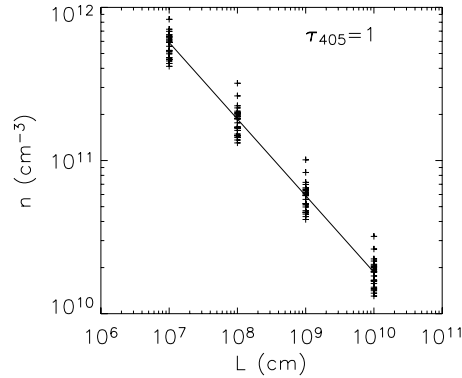
Figure 10. Density values as a function of source thickness, *L*, assuming that the source becomes optically thick at 405 GHz.

$\tau_\nu \sim \kappa_\nu L$, where L is the source thickness and κ_ν the absorption coefficient, which is a function of the source effective temperature, T_{ef} and density, n_i (Dulk, 1985).

Using the values of T_{ef} obtained earlier and supposing that $\tau_{405} = 1$, we have calculated the densities for different values of source thickness, L, ranging from 10^7 to 10^{10} cm. The result can be seen in Figure 10. This density, however, should be considered as a lower limit to the source density. Since the density is proportional to the frequency where $\tau = 1$, if the source becomes optically thick at frequencies higher than 405 GHz (which is probably the case), then the densities will be larger. Thus, the value 10^{10} cm^{-3} is considered the lower limit to the active region density. Tapping and Zwaan (2001), from a study of active region sources at 10.7 GHz, obtained electron densities of $1-2 \times 10^9$ cm^{-3} for the diffuse component. However, at this low frequency, the sources are probably located much higher in the solar atmosphere than the submillimetric counterparts.

4. Discussion and Conclusions

The main goal of this study was to perform a statistical analysis of the submillimetric emission of active regions observed in the SST solar maps as regions of enhanced brightness. The flux density spectra at 212 and 405 GHz were found to increase with frequency with a slope of 2, suggesting that the emission at these frequencies was due to thermal bremsstrahlung emission from optically thick sources. Previous works at high radio frequencies have also concluded the emission to be basically free–free emission. Tsuchiya and Takahashi (1968) from a study of a single active region concluded that the emission at 70 and 94 GHz was free–free radiation from an optically thin source. Kundu (1970) studied active regions at 33, 86, and 250 GHz and found that the observed brightness temperature enhancements seemed consistent with a thermal origin in higher-density regions at chromospheric temperatures.

On the other hand, Efanov *et al.* (1969) results of active region sources indicated that the emission at 37 and 133 GHz was thermal from an optically thick source. From observations of active regions at frequencies between 300 and 857 GHz, which emission increased with frequency, Righini-Cohen and Simon (1977) ruled out that these sources were optically thin.

Intensity enhancements of 3–17% above the emission from the solar disk were obtained at 212 GHz, that correspond to brightness temperature excess of 200–1000 K, assuming the quiet-Sun brightness temperature to be 5900 K. The lower limit of these values is in agreement with the observations by previous works at 250 GHz, namely 3% (Kundu, 1970) and 6% (Beckman and Clark, 1973). At 405 GHz, higher percentages were also found, namely 5–20% above quiet-Sun values, which are equivalent to brightness temperature enhancements of 250–1000 K, however, the adopted 5100 K for the quiet-Sun brightness temperature is lower. The lower values of these excess brightness temperature enhancements are similar to observations at 375 GHz of 6% (Beckman and Clark, 1973) and at 353 GHz that yield 11% (Bastian, Ewell, and Zirin, 1993). Here the emission from the higher frequencies radio sources were observed to be optically thick thermal bremsstrahlung, with inferred effective temperatures of $0.6–2.9 \times 10^4$ K.

The $2'–7'$ source sizes obtained from the SST maps (deconvolved assuming Gaussian sources) are compatible with values obtained for observations of active regions from other single dish telescopes at other frequencies. In particular, the size of active region 0030 (18 July 2002) is compatible with what would be observed by optical and ultraviolet telescopes with the same spatial resolution of SST. Table I lists values of $2'–7'$, as measured from previous authors for a large range of frequencies. However, these values should be taken as a composite of multiple smaller sources. Using a telescope of $31''$ angular resolution, Hachenberg, Steffen, and Harth (1978) reported the size of regions of enhanced emission at 35 GHz to be between $31''$ and $55''$. The millimetric maps at 17 and 34 GHz from Nobeyama show that the active regions are indeed composed of several smaller sources around $1'$. The submillimeter sources analyzed here appear to be of the same type as the diffuse sources reported by Tapping and Zwaan (2001) at 10.7 GHz. Our results point to a chromospheric source similar to the 10.7 GHz, however located lower in the atmosphere, because of its inferred lower temperatures and higher densities.

In summary, from a study of 23 regions of enhanced emission observed at 212 and 405 GHz, the first statistical study at such high frequencies, we have concluded the following:

- Submillimeter brightness temperature enhancements of 3–20% above quiet-Sun levels, which correspond to 200–1000 K, are associated with active regions.
- The multiple radio sources within an active region have a combined size ranging from $2'$ to $7'$.

– The overall emission from the submillimeter sources might be attributed to thermal bremsstrahlung from optically thick sources, mostly not affected by gyro-resonance effects.
– In this case, source effective temperatures are in the range of $0.6 - 2.9 \times 10^4$ K.

It would be interesting to perform the same type of analysis on the submillimeter maps after a deconvolution of the actual antenna beam is performed to look for the inner component as suggested by Tapping and Zwaan (2001). This will be the subject of a future study. Moreover, the determination of the turnover frequency requires observations with receivers at higher frequencies from which a derivation of density will be achieved. These results will yield improved atmospheric models.

Acknowledgements

References

Bastian, T. S., Ewell, M. W., and Zirin, H.: 1993, *Astrophys. J.* **415**, 364.
Beckman, J. E. and Clark, C. D.: 1973, *Solar Phys.* **29**, 25.
Buhl, D. and Tlamicha, A.: 1970, *Astron. Astrophys.* **5**, 102.
Castelli, J. P. and Clemens, J.: 1966, *Astron. J.* **71**, 652.
Costa, J. E. R. Costa, Silva, A. V. R., Lüdi, A., and Magun, A.: 2002, *Astron. Astrophys.* **387**, 1153.
Degiacomi, K., Kneubuhl, F. K., Huguenin, D., and Muller, E. A.: 1984, *Int. J. Infrared Millimeter Waves* **5**, 643.
Dulk, G. A.: 1985, *Ann. Rev. Astron. Astrophys.* **23**, 169.
Efanov, V. A., Kislyakov, A. G., and Moiseev, I. G.: 1972, *Solar Phys.* **24**, 142.
Efanov, V. A., Kislyakov, A. G., Moiseev, I. G., and Naumov, A. I.: 1969, *Solar Phys.* **8**, 331.
Hachenberg, O., Steffen, P., and Harth, W.: 1978, *Solar Phys.* **60**, 105.
Kakinuma, T. and Swarup, G.: 1962, *Astrophys. J.* **136**, 975.
Kaufmann, P.: 1968, *Solar Phys.* **4**, 58.
Kaufmann, P., *et al.*: 2001, in J. T. Pinho, G. P. S. Cavalcante, and L. A. H. G. Oliveira (eds.), *Proceedings of the 2001 SBMO/IEEE MTT-S International Microwave and Optoelectronics Conference*, Brazil, p. 439.
Kundu, M. R.: 1970, *Solar Phys.* **13**, 348.
Linsky, J. L.: 1973, *Solar Phys.* **28**, 409.
Mangum, J. G.: 1993, *PASP* **105**, 117.
Nakajima, H. *et al.*: 1994, *Proc. IEEE* **82**, 705.
Righini, G. and Simon, M.: 1976, *Astrophys. J.* **203**, L95.

Righini-Cohen, G. and Simon, M.: 1977, *Astrophys. J.* **217**, 999.
Simon, M.: 1965, *Astrophys. J.* **141**, 1513.
Tapping, K. F. and Zwaan, C.: 2001 *Solar Phys.* **199**, 317.
Tlamicha, A.: 1968, *Solar Phys.* **5**, 377.
Tsuchiya, A. and Takahashi, K.: 1968, *Solar Phys.* **3**, 346.